UNIVERSITÉ LIBRE DE BRUXELLES

DIGITAL COMMUNICATIONS

WIRELESS COMMUNICATION CHANNELS

Design of a wireless communication channel

Authors:
Anass Denguir
Luca Noël

Professors:
Philippe De Doncker
François Horlin

June 17, 2019

Contents

1 Introduction

In this project, an entire OFDM communication chain as depicted in Figure 1 will be simulated. The goal is to ensure a proper end-to-end communication by taking into account all the distortions induced by the wireless channels on the transmitted signals. For this purpose, a Single Input Single Output (SISO) OFDM communication chain will firstly be implemented in Section 2. Afterwards, the effect of multiple reception antennas will be studied by simulating a Single Input Multiple Output (SIMO) OFDM communication chain in Section 3.1.

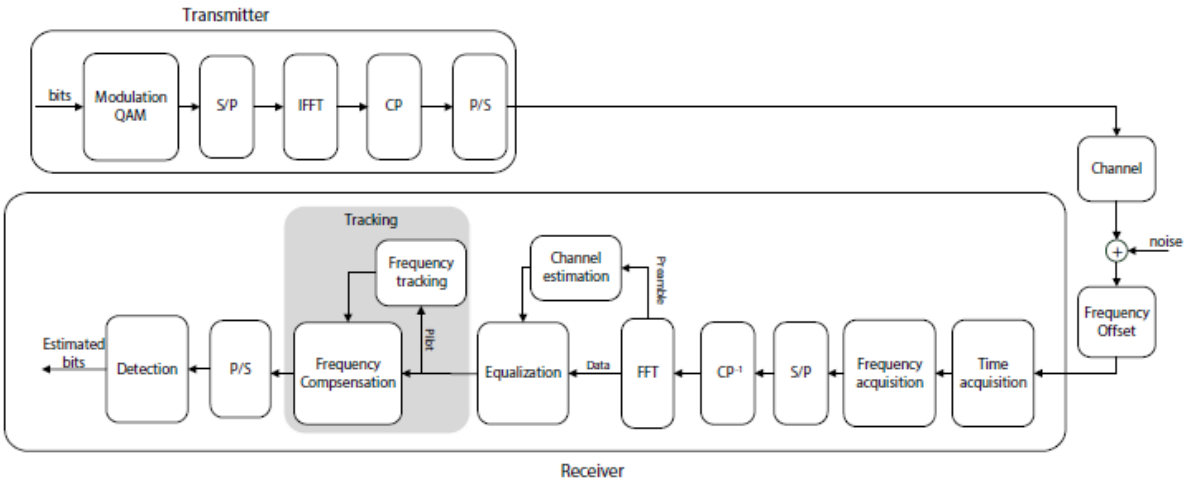

Figure 1: Block diagram of the OFDM communication chain

2 SISO Communication

2.1 Channel study

2.1.1 Transfer function and impulse response

The experimental environment is an indoor laboratory where the transfer functions of the channel have been measured at different spatial locations. The provided measurements consist of 1000 transfer functions $H_{(x,y,z)}(f)$ measured in a $10 \times 10 \times 10$ virtual array of antennas, each one separated by $2cm$. The bandwidth of interest is $[2.25, 2.45]GHz$ measured at a frequency resolution of 400 kHz. An example of such a measurement is provided in Figure 2, which corresponds to the transfer function of position $(0, 0, 0)$ in the antenna array for both LOS and NLOS configurations. One can observe in Figure 2 that the channel is frequency selective as the transfer functions $|H|$ drops for some values of the frequency f. The frequency selectivity nature of the channel is an important phenomenon present in wireless communication channel that leads to bit corruption if not taken into account.

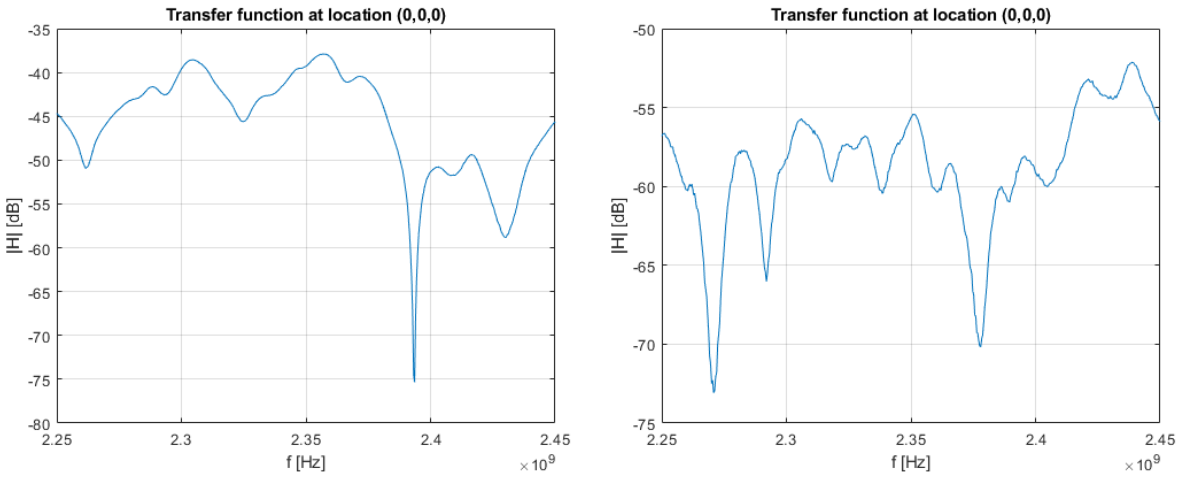

(a) LOS (b) NLOS

Figure 2: Transfer function of Channel at location $(0, 0, 0)$

In order to investigate further the channel, it is proposed to evaluate its impulse response. Under the quasi-static approximation, the channel can be considered as time invariant during the transmission of a symbol. Hence the impulse response $h(\tau)$ can be evaluated as the IDFT of $H(f)$. The impulse response is depicted in Figure 3. One can see that multiple echos of the signal are perceived at different time delays. This phenomenon, referred to as time-dispersion, causes inter-symbol interference (ISI) during communication if not taken into account. In fact, it can be shown that the frequency selectivity present in Figure 2 is a direct consequence of the time-dispersion observed in Figure 3. However, the depicted impulse response $h(\tau)$ of Figure 3 has to be corrected in order to be a real physical signal. Indeed, two corrections have to be made on this signal:

1. At the end of the impulse response, the signal is rising up. This phenomenon is due to the periodicity of the IDFT that is applied to generate $h(\tau)$ and has to be removed since no additional signal can be perceived after such a long time in an indoor environment. In practice, only the first 60 taps of the signal are kept, which corresponds to the first $300ns$. After this period, the impulse response plateaus to a value corresponding to the noise level.

2. Another phenomenon that has to be corrected in the impulse response is the transient effect that appears at the beginning of the curve. This effect is due to the finite bandwidth of the measuring system. This is not expected since the first perceived signal should be the one corresponding to the maximum value of h. Hence, the parts of the curve situated before the maximum can be discarded.

The corrected impulse responses are shown in Figure 4 for both LOS and NLOS cases. As expected, the values of the impulse response are higher in LOS configuration. This is due to the fact that the LOS ray carries a lot of energy.

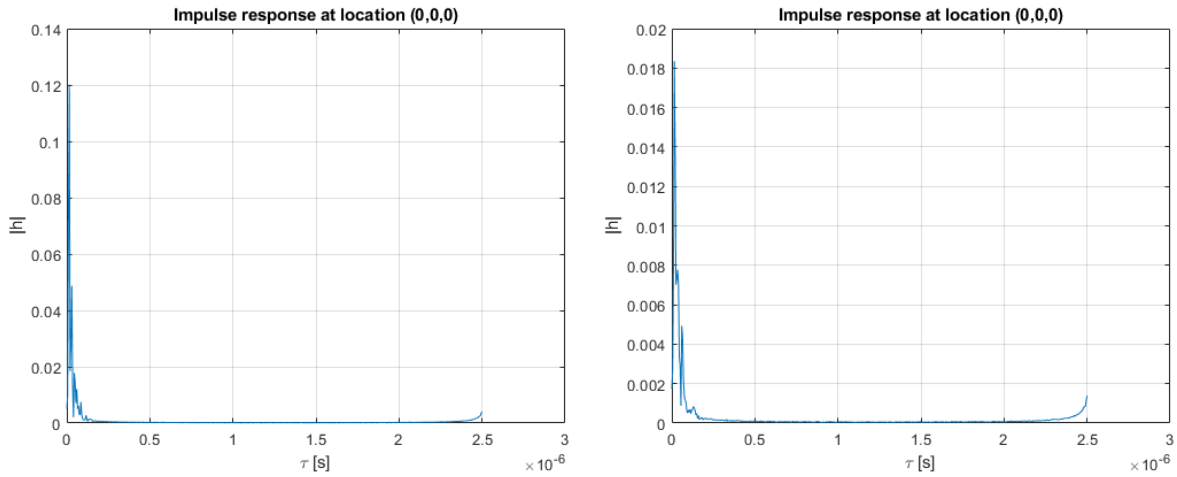

(a) LOS (b) NLOS

Figure 3: Transfer function of Channel at location $(0, 0, 0)$

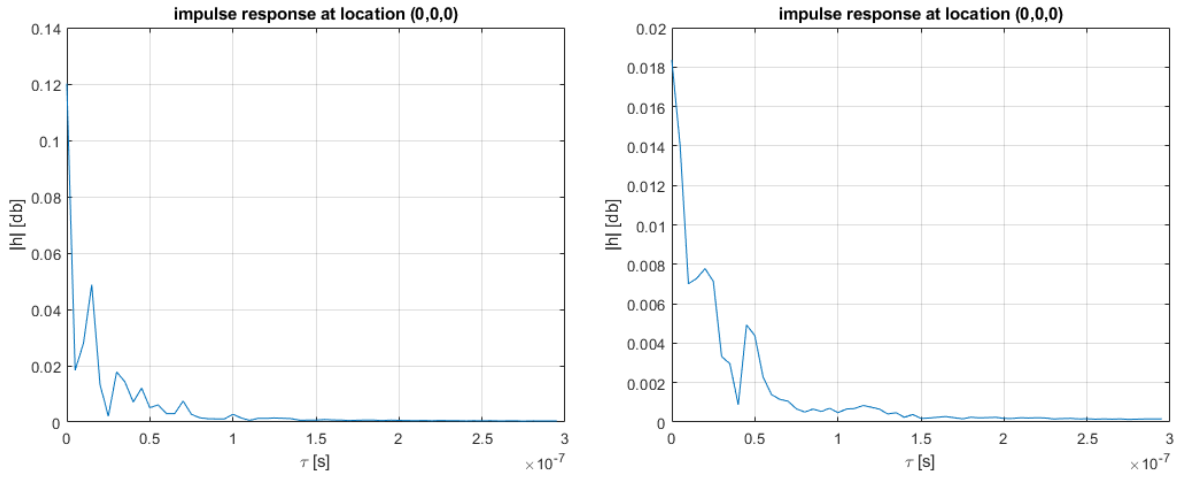

(a) LOS (b) NLOS

Figure 4: Impulse response of the $200MHz$ channel at location $(0, 0, 0)$

2.1.2 Power Delay Profile and Coherence bandwidth

The Power Delay Profile can be computed for each tap τ by averaging the squared value of the impulse response at each spatial coordinate (x, y, z) of the virtual antenna array. This is expressed in equation 1. The experimental PDP are illustrated by the blue curves in Figure 5 where it clearly appears that the power obtained at the reception is dispersed in time. One can also notice the power gain in the LOS case compared to the NLOS ($\sim 10\ dB$).

$$P(\tau) = \frac{1}{N_x N_y N_z} \sum_x \sum_y \sum_z |h_{(x,y,z)}(\tau)|^2 \tag{1}$$

From this knowledge, the delay spread σ_τ can be derived using equations 2, 3 and 4. The delay spread is a quantity that evaluates the time dispersion of the channel. The higher the delay spread, the more time we have to wait before sending a symbol in the channel in order to avoid ISI. The values of the delay spread for both LOS and NLOS scenarios are shown in the first column of Table 1.

$$\sigma_\tau = \sqrt{\frac{1}{P_T} \int_0^\infty \tau^2 P(\tau) d\tau - \tau_m^2} \tag{2}$$

$$P_T = \int_0^\infty P(\tau) d\tau \tag{3}$$

$$\tau_m = \frac{1}{P_T} \int_0^\infty \tau P(\tau) d\tau \tag{4}$$

In practice, the PDP can be well approximated by formula 5, which is represented by the red curves in Figure 5. Therefore, we can conclude that the PDP drops exponentially until reaching the noise floor.

$$P(\tau) = P(0)\, e^{-\tau/\sigma_\tau} \tag{5}$$

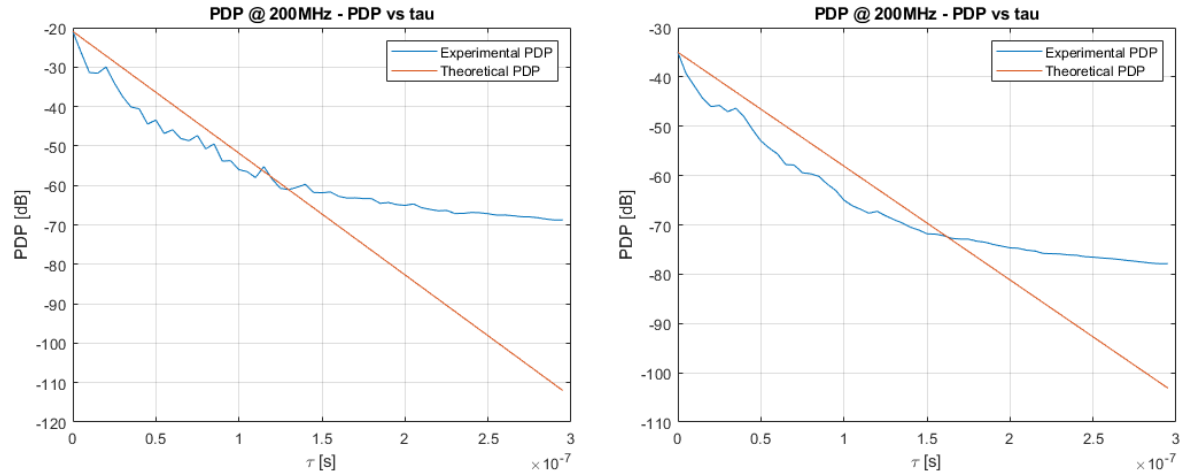

(a) LOS (b) NLOS

Figure 5: PDP of the system with $BW = 200MHz$

Another quantity that can be analyzed is the coherence bandwidth Δ_{fc} of the channel. This is expressed in equation 6. The coherence bandwidth measures the frequency range over which the transfer function $H(f)$ can be considered as a flat channel. Therefore, if the bandwidth of the communication channel BW is lower than Δ_{fc}, the entire

channel frequency response can be considered as flat and no time dispersion (and no ISI) happens. Delay spread and coherence bandwidth are thus dual quantities that express the same idea respectively in time and frequency domain. The measured values of the coherence bandwidth are reported in the second column of Table 1.

$$\Delta_{fc} = \frac{1}{2\pi\sigma_\tau} \tag{6}$$

	σ_τ	Δ_{fc}
NLOS	17.44 ns	9.12 MHz
LOS	12.55 ns	12.68 MHz

Table 1: Delay spread and Coherence bandwidth for $BW = 200MHz$

2.1.3 Impact of the system bandwidth on the impulse response

Until now the results presented were obtained by considering a system bandwidth of $200MHz$. It is proposed to study the effect of a bandwidth reduction by a factor 10 on the impulse response and the PDP. This corresponds to reducing the system bandwidth to $20MHz$. Therefore, a rectangular window of observation of length $20MHz$ and centered on $f_c = 2.35GHz$ must be applied on the transfer functions of Figure 2. In the time domain, this operation provides a downsampled version of the impulse response of Figure 4 by a factor 10. The obtained $6 - taps$ impulse responses are depicted in Figure 6 and the effect on the corresponding PDP is illustrated in Figure 7. The delay spread and the coherence bandwidth are reported in Table 2 for both LOS and NLOS scenarios. These values are very close to those of Table 1 because these quantities are intrinsic characteristics of the channel which do not depend on the measuring system. However, a consequence of the system bandwidth reduction is that the coherence bandwidth has the same order of magnitude as the system bandwidth: $\Delta_{fc} \sim 20MHz$. Therefore, in the next section, 2 channel models will be studied:

1. the narrowband model: This model considers that all the echos of the transmitted signal fall into one single tap. In practice, this assertion is true if $BW << \Delta_{fc}$.

2. the wideband model: This model will consider that the echos of the transmitterd signal fall into the 6 taps present in Figure 6, where each tap appears every 50 ns.

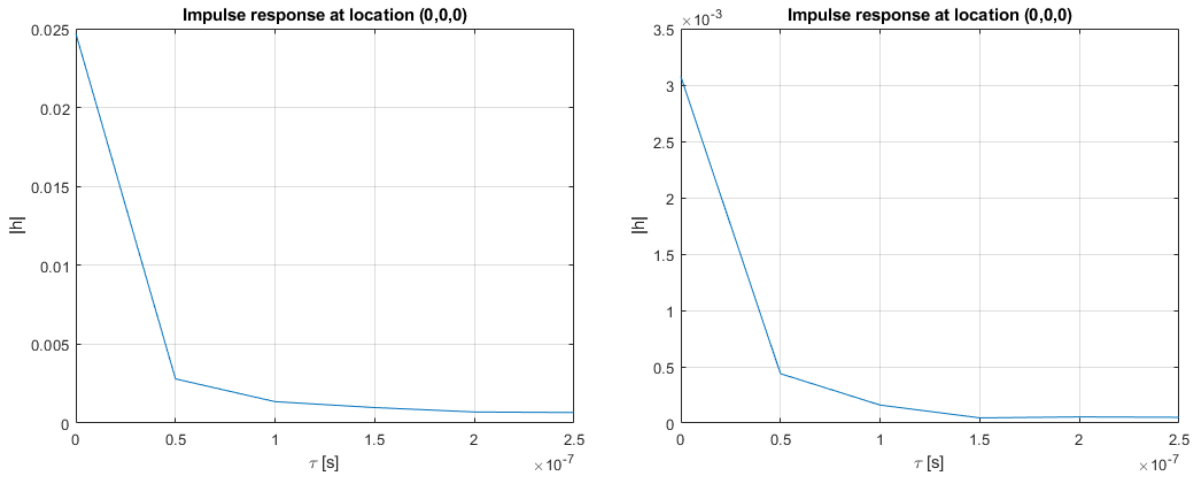

(a) LOS (b) NLOS

Figure 6: Impulse response of the $20MHz$ channel at location $(0, 0, 0)$

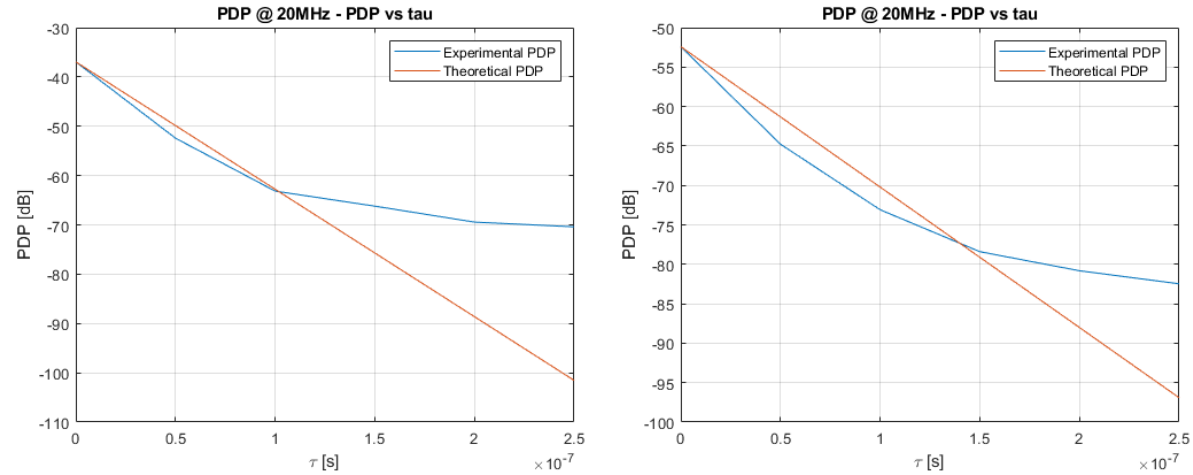

(a) LOS (b) NLOS

Figure 7: PDP of the system for $BW = 20MHz$

	σ_τ	Δ_{fc}
NLOS	18.99 ns	8.38 MHz
LOS	12.75 ns	12.48 MHz

Table 2: Delay spread and Coherence bandwidth for $BW = 20MHz$

2.2 Narrowband and wideband model

2.2.1 Narrowband model

In the narrowband model, the receiver cannot distinguish all the arriving MPCs. Therefore, the MPCs are all falling into a single tap. The narrowband impulse response $h_{narrow}(n)$ is thus calculated for each position (x, y, z) by summing up the wideband impulse response $h_{wide}(n)$ (see Figure 6) at each tap n.

To be able to design the communication between transmitter and receiver, the stochastic distribution of the channel needs to be studied. It is proposed here to compare the statistical distributions of both narrowband and wideband models. The Figure 8 shows the probability density functions in the LOS and NLOS cases of the narrowband channel impulse response amplitude $|h|$. The PDFs are fitted with Rayleigh and Rice probability density functions. It can be shown that the narrowband channel impulse response follows a Rice distribution in the LOS case and a Rayleigh distribution in the NLOS case. In the NLOS case, the matching with both Rice and Rayleigh density functions is expected since the Rayleigh distribution is a special case of Rice distribution. In the LOS case, the PDFs only matches the Rice distribution (blue fit). The Rice distribution is characterized by a K factor which expresses the contribution of the line-of-sight component of the signal compared to the mean power of the MPCs. The definition of the K factor is detailed in equation 7. The NLOS case, as its name indicates, do not have any line-of-sight component. Hence, the K factor in this situation is equal to 0, which corresponds to a Rayleigh distribution.

$$K = \frac{a_0^2}{\sum_{i=1}^{N} a_i^2} \tag{7}$$

The K factor of both fitting Rice distributions in Figure 8 are summarized in Table 2.2.1. In the NLOS situation, the value of K is expected to be 0 but it is seen that it is not exactly equal to 0. This indicates that a small LOS component is present. The statistical study of the distribution allows the deduction of the stochastic narrowband model of the channel.

	LOS	NLOS
K [dB]	4.76	-10.51

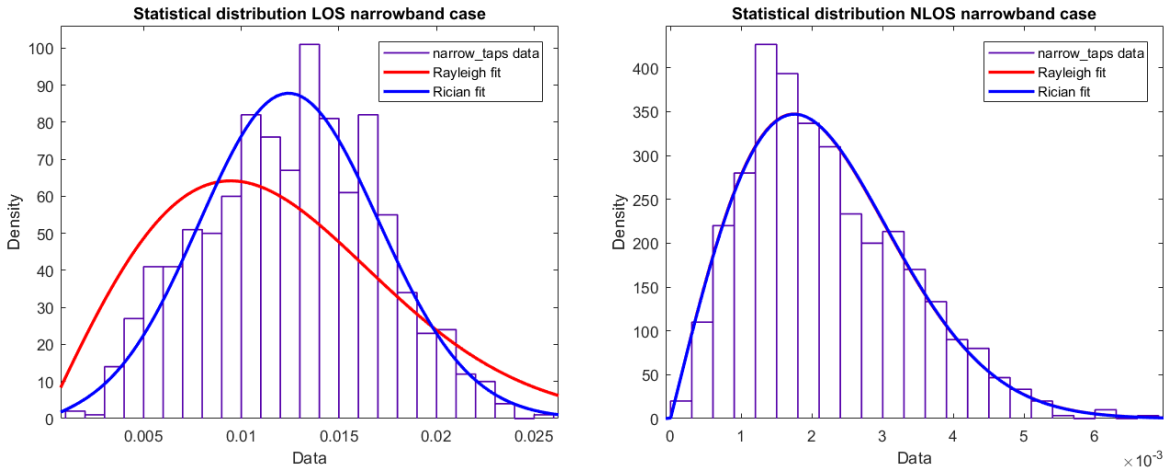

(a) LOS (b) NLOS

Figure 8: Statistical distribution for the narrowband case

2.2.2 Wideband model

The stochastic wideband model of the channel can be deduced by studying the statistical distribution of each tap of the wideband channel. Once again, the study is done in the LOS and NLOS cases. In the context of a LOS communication, it is expected that the distribution follows a Rice distribution, while the NLOS case is expected to follow a Rayleigh distribution. This is confirmed for the first tap $n = 1$ in both cases with Figure 9. For the following taps, however, the local area mainly receives echos which implies that the LOS component becomes less significant. Therefore, the distributions for the following taps $n = 2, ..., 6$ follow a Rayleigh distribution as shown in Figure 10.

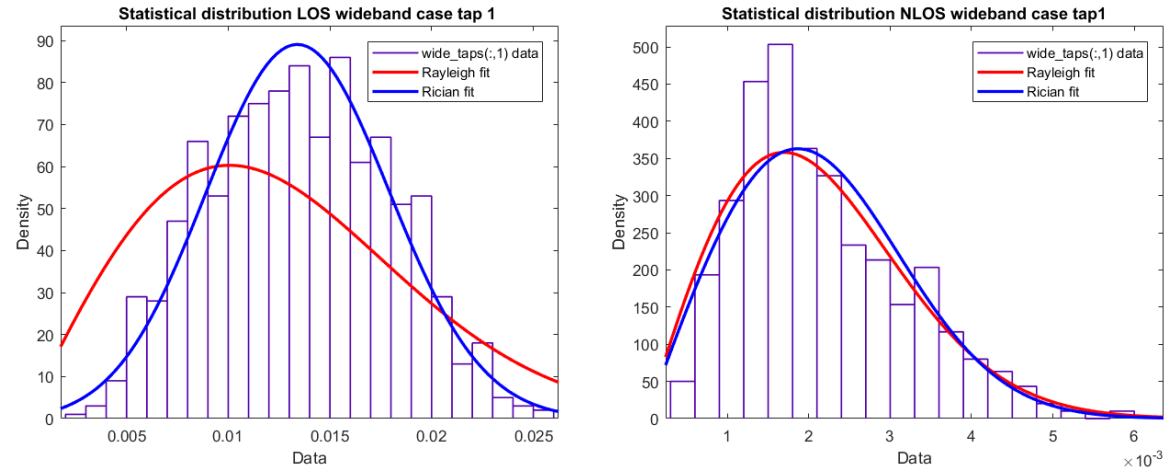

(a) LOS (b) NLOS

Figure 9: Statistical distribution for the wide-band case: tap 1

Figure 11 illustrates the evolution of the K factor at each delay tap. The LOS case shows some increase of the K factor from tap 2 to tap 3, which is unexpected. Some LOS components seems to arrive at some higher delay taps. However, the most dominant LOS component has arrived at the first tap.

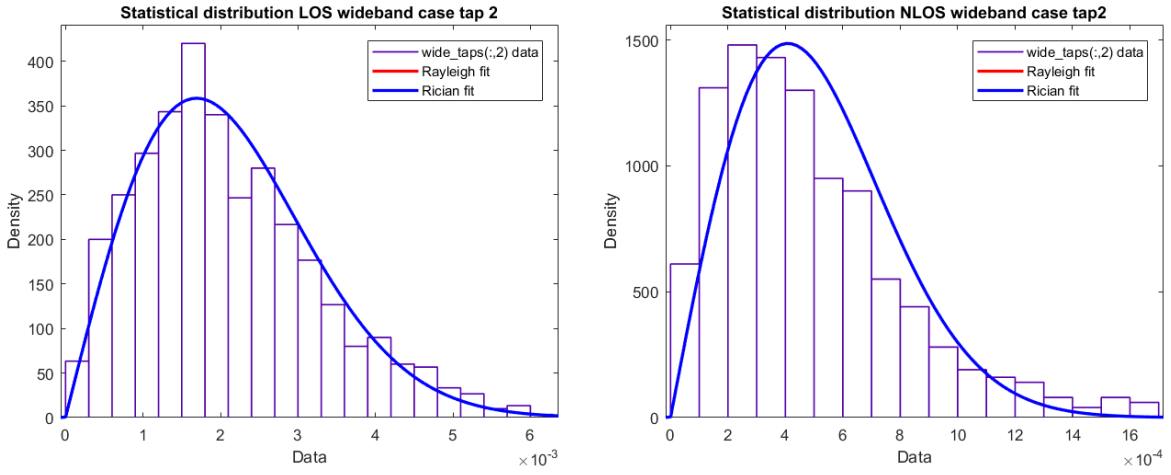

(a) LOS (b) NLOS

Figure 10: Statistical distribution for the wide-band case: tap 2

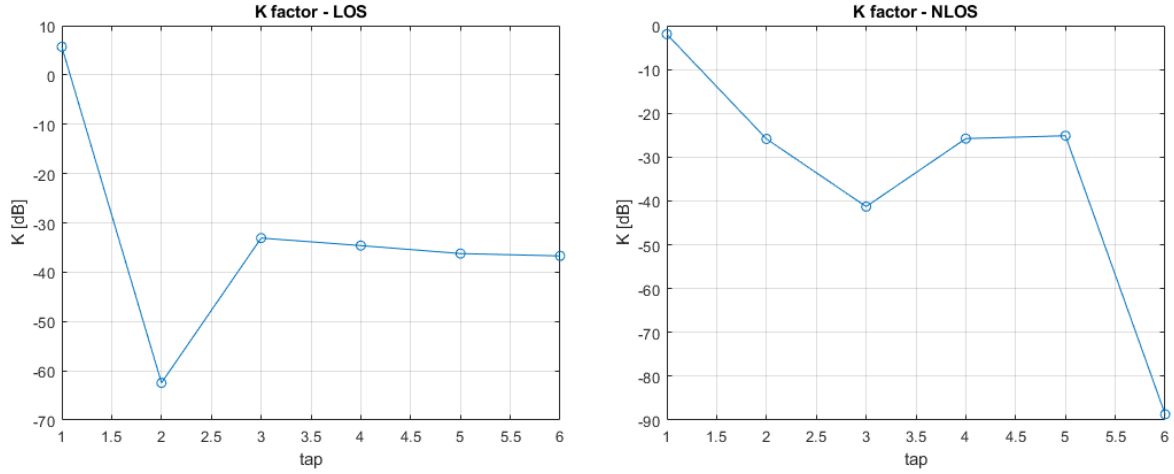

(a) LOS (b) NLOS

Figure 11: Evolution of the K factor

2.3 Channel equalization

2.3.1 OFDM

In order to recover the transmitted symbols at the receiver side, the distortions induced by the channel must be compensated. This operation is referred to as channel equalization. In this section, an OFDM communication is established to facilitate the channel equalization. The OFDM transceiver is responsible for achieving a communication on a multi-path channel. To do that, the wideband frequency selective channel is divided into N sub-channels that are narrowband frequency flat. The symbols sent by the transmitter are then transmitted by orthogonal narrowband sub-carriers.

A simplified diagram of the OFDM communication chain is illustrated in Figure 12. The bitstream at the input of the transmitter undergoes a QAM modulation. This bitstream is mapped into QAM symbols in the frequency domain. These symbols are divided into blocks of N symbols where each symbol is assigned to a flat frequency sub-channel. Each N-symbol block is converted into time domain symbols by applying an N-point IFFT on each block. Before transmitting the symbols, a Cyclic Prefix is added at the beginning of each block to be sent. The role of the cycle prefix will be explained later. Finally, the blocks are serialized and transmitted into the channel as time domain symbols.

At the receiver side, the symbols are distorted by the channel and corrupted by noise. Each received symbol is attributed to its belonging sub-carrier. The Cyclic Prefix is removed and the received symbols are converted back into frequency domain by applying an FFT. As each sub-carrier are orthogonal, the channel equalization can be performed on the symbols of each sub-carrier independently. The equalization is detailed in Section 2.3.2. Once the channel equalized, the frequency domain symbols can be serialized and mapped to their corresponding bit sequence.

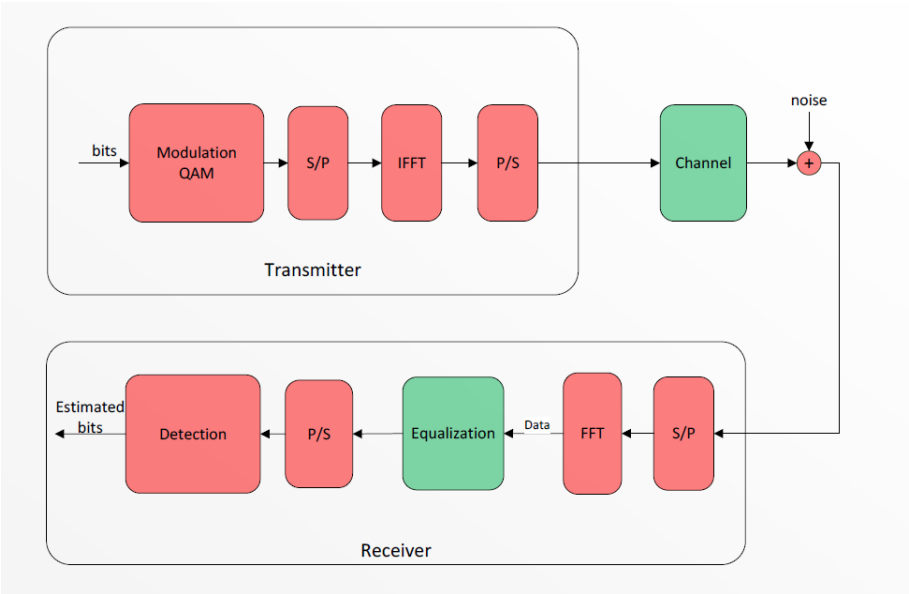

Figure 12: Block diagram of the communication chain

2.3.2 Equalization

The received signal $r(n)$ is characterized by equation 8. It is the result of the convolution of the time domain symbol with the channel. This convolution models the channel memory (i.e the presence of MPC). An additive Gaussian noise must be added to the result. In this formula, $h(n)$ is the stochastic wideband model of the channel. The time-domain symbols are represented by the term $s(n)$ and the noise is represented by $w(n)$.

$$r(n) = h(n) * s(n) + w(n) \tag{8}$$

In the frequency domain, this equation can be translated into the following equation.

$$R(k) = H(k)S(k) + W(k) \tag{9}$$

Equation 9 is useful for the equalization step of the communication chain. It shows that the QAM symbols can be recovered if the channel frequency response is known for each sub-carrier k. The sent symbols $S(k)$ are found by solving equation 10.

$$\frac{R(k)}{H(k)} = S(k) + \frac{W(k)}{H(k)} \tag{10}$$

2.3.3 Cyclic Prefix

In this section, the role of the Cyclic Prefix added on the transmitted signals will be investigated further. The Cyclic Prefix (CP) is the replication of the last part of a block of symbol, placed at the beginning of the latter. This is illustrated in Figure 13(a). The prefix is needed since equation 9 only works for periodic signals $s(n)$. This requires an infinitely long signal which is not practically possible. But since the channel impulse response has a finite size L, all the period of $s(n)$ is not needed to simulate periodicity. Only the last L_{CP} symbols placed at the beginning of the block are needed to compute the resulting signal and to simulate the periodicity of the signal. Therefore, the CP addition restores orthogonality among sub-carriers on a multi-path environment.

The CP is also used to prevent interference between blocks since the channel has a memory effect on the signal. The convolution gives $L - 1$ additional samples to the resulting signal. These samples will interfere with the CP of the following block. Therefore the size of the CP (L_{CP}) must be bigger than the size L of the channel (i.e. the duration of the Cyclic Prefix has to be longer than the delay spread) to avoid interference between data blocks. As the interference are only corrupting the CP symbols, it is told that the Cyclic Prefix acts as guard margin that avoids inter-block interference (IBI). This situation is illustrated in Figure 13(b). The effect of the CP on the bit error rate (BER) is illustrated in Figure 14, which represents the BER curves of a LOS communication with and without CP. At the beginning, the effect of the noise is dominant over IBI. Therefore, the two curves follow approximately the same evolution. However, when the value of EbN0 reaches $10dB$, the BER plateaus in the absence of CP. This is explained by the fact that the interference between blocks of symbols is becoming dominant.

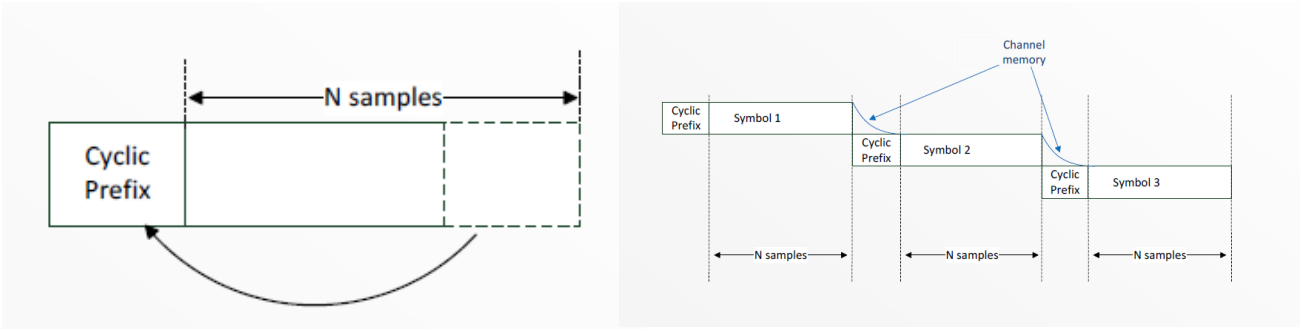

(a) Cycle prefix: principle

(b) Placement of cycle prefix

Figure 13: Cycle prefix

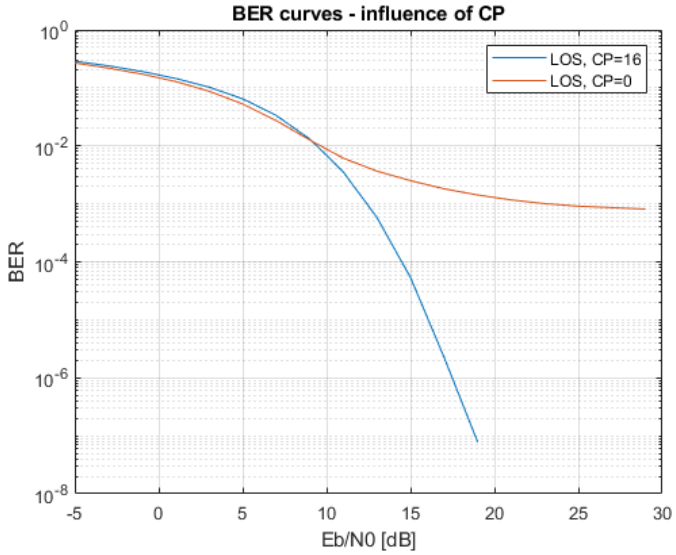

Figure 14: BER with and without CP

2.3.4 Impact of the noise on the channel

As mentioned before, the symbols are also corrupted by Additive White Gaussian Noise during the communication. The noise is modeled by the variable $W(k)$ in equation 10. The BER curves are compared in Figure 15 in the case of a LOS, NLOS and purely noisy communication channels. The sent symbols are recovered by applying a zero-forcing equalization in equation 10, which corresponds to solving this equation by setting $W(k) = 0$. Hence, the error of the equalization is quantified by the quotient $\frac{W(k)}{H(k)}$, where the transfer function $H(k)$ is supposed to be known at the receiver side. As the channel is frequency selective, some component of the noise will be divided by a high factor and others by a low factor. In the case where the factor $H(k)$ is low, the error made by the zero-forcing equalization becomes significant. Hence, the LOS channel performs better than NLOS in terms of BER because its transfer function is

higher in magnitude. The AWGN channel performs even better than LOS because it assumes a perfect communication channel, which implies no noise amplification.

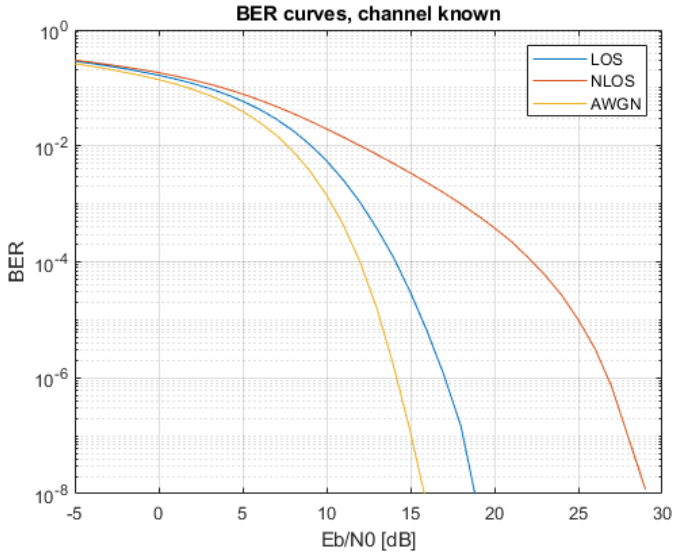

Figure 15: BER for LOS, NLOS and AWGN channel

2.3.5 Impact of the channel and modulation parameters on the channel

From the previous discussions, the following statements can be made about the design of a wireless communication chain:

- The channel transfer function is constant over the bandwidth if the coherence bandwidth Δf_c is higher than the system bandwidth BW. It is frequency selective in the other case and therefore subject to ISI.
- The delay spread σ_τ is the dual quantity of the coherence bandwidth. If the symbol duration T_S is higher than the delay spread, the channel is considered as a flat fading channel (the MPC are not distinguished). It is a frequency selective channel in the other case.
- A flat fading channel can be obtained by decreasing the system sampling frequency f_s. But this is at the expense of a lower data rate.
- In OFDM, the number of channels N, and by extend the block size, must be chosen such that each sub-channel experiences flat fading.
- In order to avoid IBI, the cycle prefix length must be higher than the delay spread σ_τ since the samples are affected by past of the signal up to duration σ_τ.

In this project, the parameters of Table 3 have been used. 64 sub-carriers are taken into account for a bandwidth of 20 MHz. Hence, each sub-channel has a bandwidth equal to 0.3125 MHz. From Table 1, the coherence bandwidth is estimated to 9.12 MHZ in the NLOS case and to 12.68 MHz in the LOS channel. Therefore, the coherence

bandwidth $\Delta f_c >> 0.3125MHz$. This confirms that each sub-carrier is affected by a narrowband channel.

Parameter	Value	Description
N	64	Number of subcarriers
L	6	Channel memory
L_{CP}	16	Length of Cyclic Prefix
BW	20 MHz	System bandwidth

Table 3: Channel and modulation parameters

2.3.6 Channel estimation

At this moment, it was assumed that the receiver knows the channel transfer function. In practice, the channel must be estimated at the receiver. This estimation is performed based on a known N-symbol block referred to as the preamble. This preamble is built is the frequency domain by generating a random sequence of +A and -A symbols, where the value of A is chosen so that the preamble has the same power as the data symbols. This is expressed in equation 11 where M is the number of sent symbols and s_i is the i^{th} symbol in the frequency domain.

$$A = \sqrt{\frac{1}{M}\sum_{i=1}^{M}|s_i|^2} \tag{11}$$

As depicted in Figure 16, two preambles are placed at the beginning of the symbol frame in time domain and are prefixed by a CP of size 32. The preamble will be used to estimate the channel at the receiver by computing equation 12, where $S'(k)$ is the frequency spectrum of the preamble symbols and $R'(k)$ is the received preamble symbol spectrum. The channel estimation is based on the averaged estimation of both preamble symbols. The reason of the presence of two replications of the same preamble symbols will be explained later.

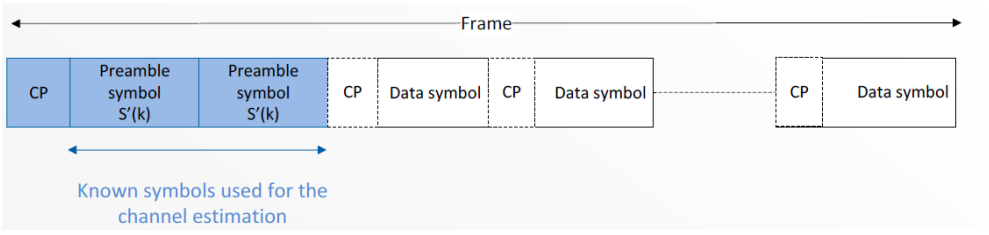

Figure 16: Frame structure

$$\hat{H}(k) = \frac{R'(k)}{S'(k)} = H(k) + \frac{W(k)}{S'(k)} \tag{12}$$

The BER is computed for the LOS channel and NLOS channel. A comparison between the two scenarios is made in Figure 17. The first scenario is the case where the

receiver knows the exact value of the channel impulse response. The second scenario is where the channel is estimated from the knowledge of the preamble. When applying zero-forcing equalization, the error on the channel estimation is $\frac{W(k)}{S'(k)}$. Hence the error on the received symbol is amplified.

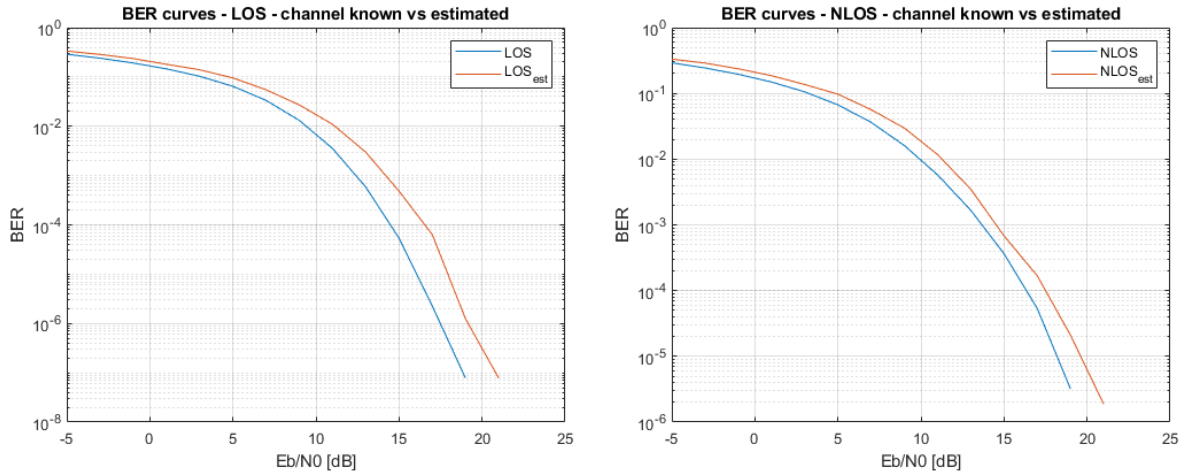

(a) LOS (b) NLOS

Figure 17: Comparison of BER for the known channel case and the estimated channel case

The accuracy of the channel estimate is quantified by the normalized mean squared error of equation 18. It can be shown that the NMSE decreases as the SNR increases.

$$NMSE = \frac{\sum_k |\hat{H}(k) - H(k)|^2}{\sum_k |H(k)|^2} \tag{13}$$

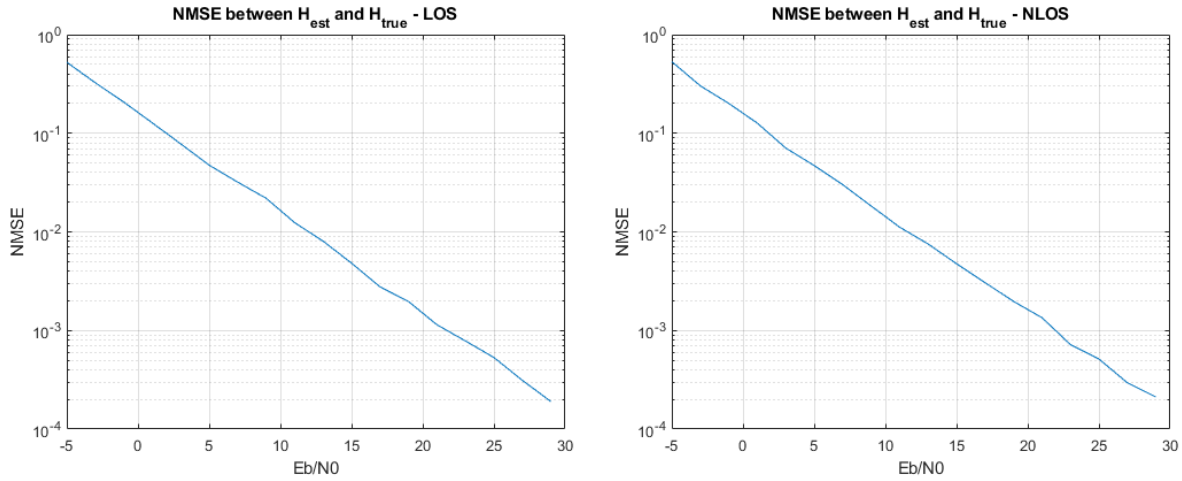

(a) LOS (b) NLOS

Figure 18: NMSE

2.4 Synchronization

2.4.1 Time of Arrival

In a real communication, one cannot distinguish the beginning of a symbol frame unless the time-of-arrival (ToA) of this frame is estimated. Hence, the time-of-arrival (ToA) of the data stream is evaluated by spotting a known preamble in the symbol frame. But the evaluation of the ToA yields some uncertainty on the ground truth time-of-arrival.

Let's suppose that the ToA is estimated too early compared to the real ToA. The FFT at the receiver is performed on a part of the CP and its respective data symbols. The CP is basically the last 16 symbols taken from its corresponding 64 symbols block. This is situation is depicted in Figure 19(a). A right circular shift, in the time domain, affects the received symbols and corresponds to multiplying the data spectrum with an exponential in the frequency domain. The FFT applied on the data symbols at the receiver can be expressed as follows:

$$s(n + n_0) \mapsto S(k)e^{-j2\pi \frac{k}{N} n_0} \tag{14}$$

S and s refers to the emitted data block in frequency domain and the data block in the time domain respectively. The effect of ToA is a phase shift on the data spectrum that depends on the subcarrier. The phase shift is compensated at the channel estimation step and the equalization step, because the time-of-arrival is measured as a part of the channel.

$$R(k) = H(k)S(k)e^{j\Phi(k)} + W(k) \tag{15}$$

The channel estimation based on preamble S'(k) is expressed as follows:

$$\hat{H}(k) = \frac{H(k)S'(k)e^{j\Phi(k)} + W(k)}{S'(k)} = H(k)e^{j\Phi(k)} + \frac{W(k)}{S'(k)} \tag{16}$$

The channel estimation takes into account the phase shift introduced by the ToA. This phase shift is compensated during equalization.

If the estimation of the ToA is later than the real ToA, the FFT is performed on the data block and on a part of the following block CP. This situation is depicted in Figure 19(b). Inter Block interference is then introduced which deteriorates the communication performance. If not compensated, the ToA should stay smaller than the cycle prefix length in order to avoid IBI.

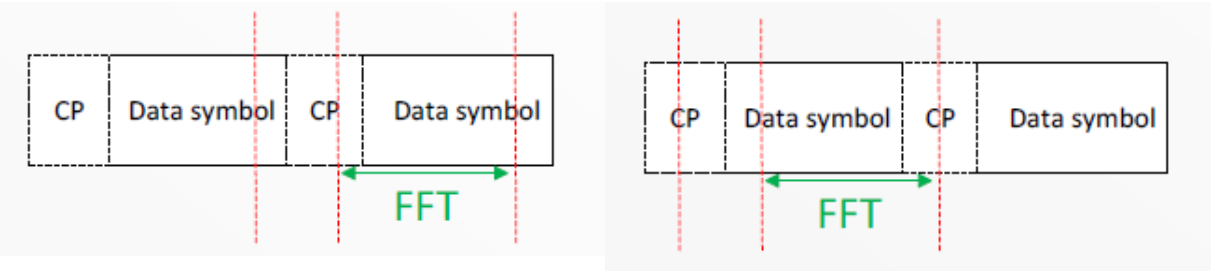

(a) Too early

(b) Too late

Figure 19: Estimation of Time-of arrival

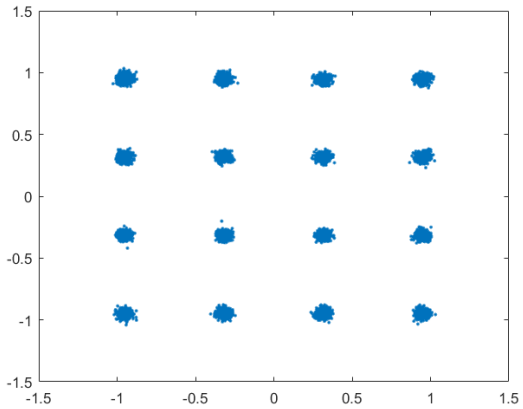

Figure 20: Received symbols before equalization - AWGN case - ToA = 0

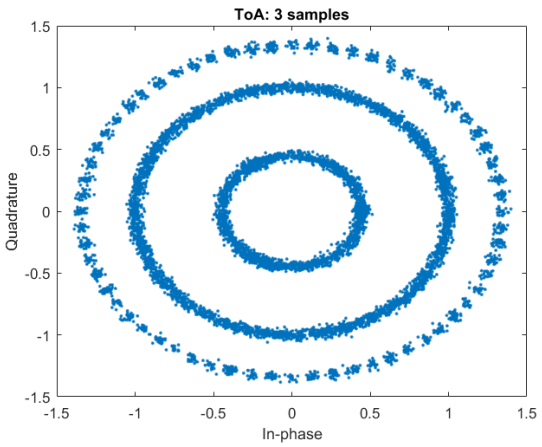

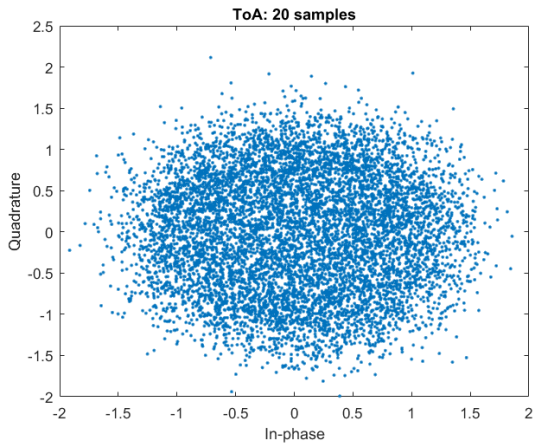

(a) ToA impact on received symbols: 3 samples

(b) ToA impact on received symbols: 20 samples

Figure 21: Impact of ToA on constellations

A time acquisition mechanism has to be implemented in order to compensate the ToA on the received signal. The ToA is expressed in term of number of samples. We exploit the fact that there are two redundant preambles at the beginning of the serialized signal. The auto-correlation of the sequence received is computed for each time n between a block of size N and another block of the same size at time n+N. The auto-correlation yields a curve with a plateau of length $2CP + 1$ where 2 CP is the size of the CP from the preamble. This is depicted in Figure 22. The plateau gives the maximum correlation at the sample numbers corresponding to the CP preamble. However, the value of the ToA can not be directly deduced from this plateau since, for several value of n, the correlation gives a maximum value. Therefore, the auto-correlation undergoes a moving average. The moving average is done with a window of size $2CP + 1$ since this is the size of the plateau. This will give one maximal value for the auto-correlation, whose time index is considered as the estimated ToA.

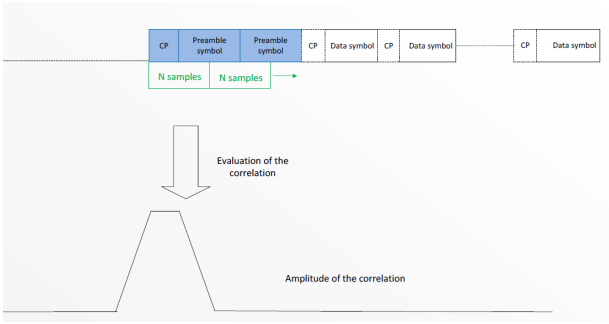

Figure 22: Auto-Correlation

The effect of the ToA on the received symbols is shown in Figures 20 and 21 in the case of an AWGN channel. In Figure 20, one can observe the QAM symbols that are supposed to be received in case of no synchronization error. The effect of the phase shift introduced by the ToA is illustrated in Figure 21. In the left situation, the ToA is smaller than the CP and hence do not influence the performance. This is because the data symbols are shielded by a 16-sample CP that avoid IBI. In the right figure, the ToA reaches 20 samples, introducing then IBI.

It is proposed now to estimate the accuracy of the ToA estimation. From Figure 23, it appears that the ToA estimation becomes more accurate for high SNR value. Indeed, since symbol blocks are distorted independently, if the noise level is high the two blocks composing the preamble will be uncorrelated. Hence, the auto-correlation will not yield a satisfying ToA.

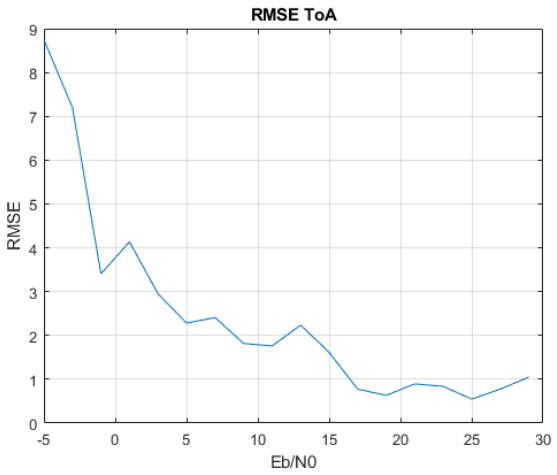

Figure 23: ToA accuracy expressed as RMSE

Figure 24(a) shows, in blue, a BER curve for a ToA equal to zero and, in red, the BER curve when a non compensated ToA of 20 samples is present. The ToA compensation corrects the synchronization error as depicted in Figure 24(b). The compensation allows to keep up a BER performance almost equal to the no ToA case.

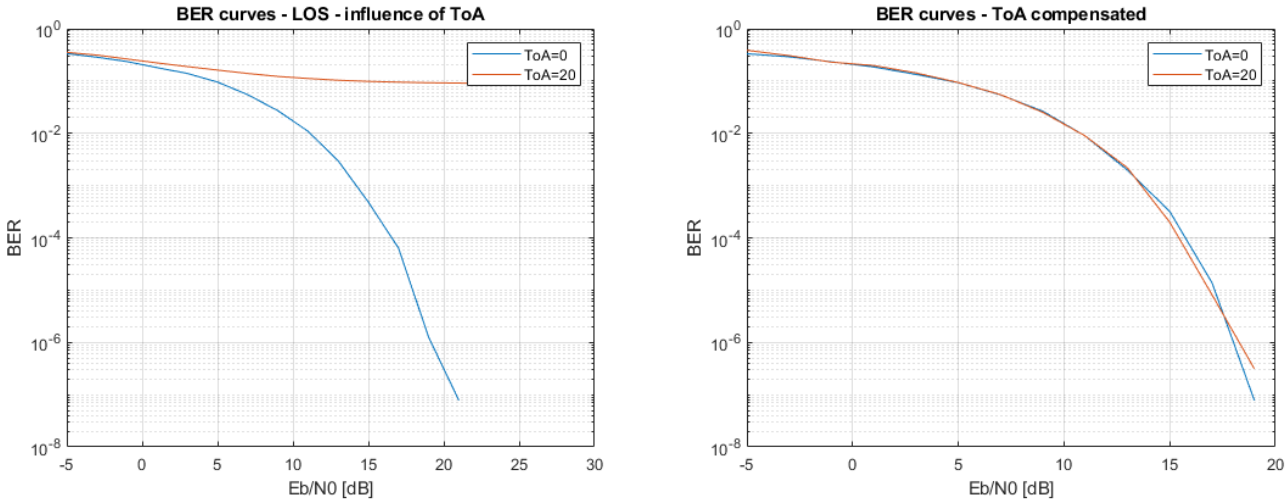

(a) ToA not compensated

(b) ToA compensated

Figure 24: Impact of ToA on BER performance - ToA = 20 samples

2.4.2 Frequency acquisition

In practice, the OFDM communication is affected by a CFO, carrier frequency offset.

The accuracy of oscillators at transmitter and receiver is limited. Therefore, a difference of carrier frequency at both side can be highlighted.

$$r(t) = s(t)e^{j2\pi f_{TX}t}e^{-j2\pi f_{RX}t} = s(t)e^{j2\pi(f_{TX}-f_{RX})t} \tag{17}$$

In discrete time:

$$r(n) = s(t)e^{j2\pi(f_{TX}-f_{RX})nTs} \tag{18}$$

The CFO induces a progressive phase rotation to the baseband signal. This phase rotation can be observed in Figure 25, where the impact of the CFO on the constellation diagram is shown for a fixed number of sent symbols. The more symbols sent, the higher the phase shift since the latter evolves with time at a rate imposed by the CFO. As expected, the BER is deteriorated by high CFO values. This shown in Figure 26.

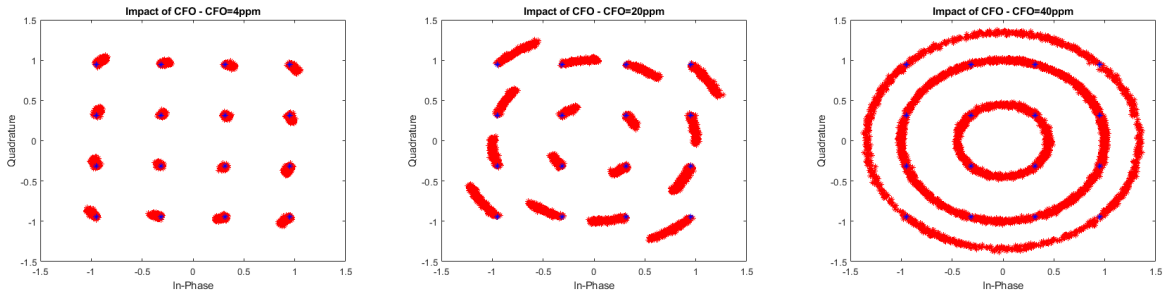

(a) CFO=4ppm (b) CFO=20ppm (c) CFO=40ppm

Figure 25: Impact of CFO on constellation

To compensate the effect of the CFO on the received symbols, a frequency acquisition is performed. The frequency acquisition is based on the preamble. It is important that the CFO estimation is done after time acquisition since the frequency acquisition requires the correct preamble. The frequency acquisition is done by comparing the phase of the first preamble block with the following preamble block. The CFO is estimated as follows.

$$CFO = \frac{\angle r2^{*}r1}{2\pi NT_s} \tag{19}$$

Where $(r2^{*}r1)$ denotes the correlation between the first preamble block and the second preamble block, N is the preamble block size.

The CFO acquisition is a rough compensation of the true CFO. When the accuracy of the frequency acquisition is considered sufficient, the ICI (inter carrier interference) can be considered negligible. It can be shown that the CFO deteriorates the BER performance but the symbols sent by the transmitter can still be recovered with a high

enough SNR.

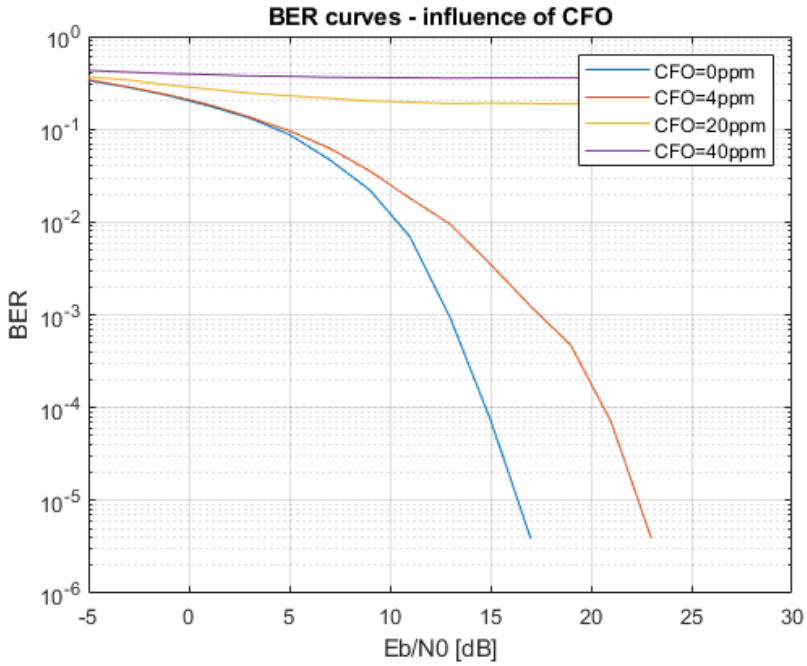

Figure 26: Impact of CFO on BER curves for different value of CFO

The CFO acquisition has a limited range of CFO that can be compensated. The angle found with the frequency acquisition can be expressed as $\Delta\phi = \Delta\phi + 2k\pi$ where k is an integer. If the phase difference exceeds 2π, the estimation of the CFO could be incorrect. The maximum CFO that can be compensated is found by resolving inequation 20.

$$\Delta\phi = 2\pi\Delta f_{max} N T_s < 2\pi \tag{20}$$

Hence the CFO is limited to Δf_{max}

$$\Delta f_{max} < \frac{1}{NT_s} \tag{21}$$

Knowing that the block size N is equal to 64 and the symbol frequency is 20 MHz.

$$\Delta f_{max} < 312.5kHz \tag{22}$$

After the frequency acquisition, a frequency tracking must be done since the CFO estimation is only a rough estimation. As shown in Figure 27, the tracking is done by checking the phase rotation of pilot symbols done during communication. Pilot symbols are known symbols that are inserted on specific frequency channels of each OFDM signal. The residual CFO is tracked by averaging the phase rotations of the pilots symbols at the receiver side.

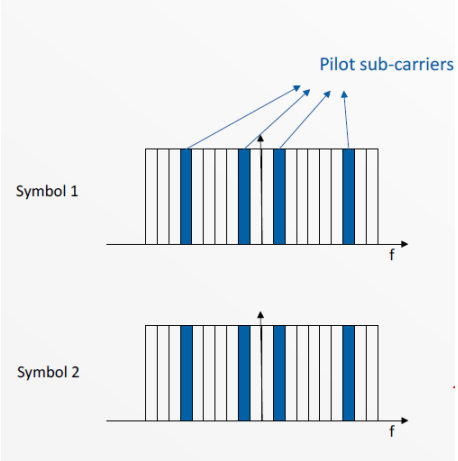

Figure 27: frequency tracking with pilot symbols

We can see the effect of frequency acquisition and frequency tracking on the BER performance in Figure 28. The values of CFO are corrected successfully and the BER performances are improved compared to Figure 26. It is expected since the role of frequency tracking is to correct residual errors left by the CFO estimation.

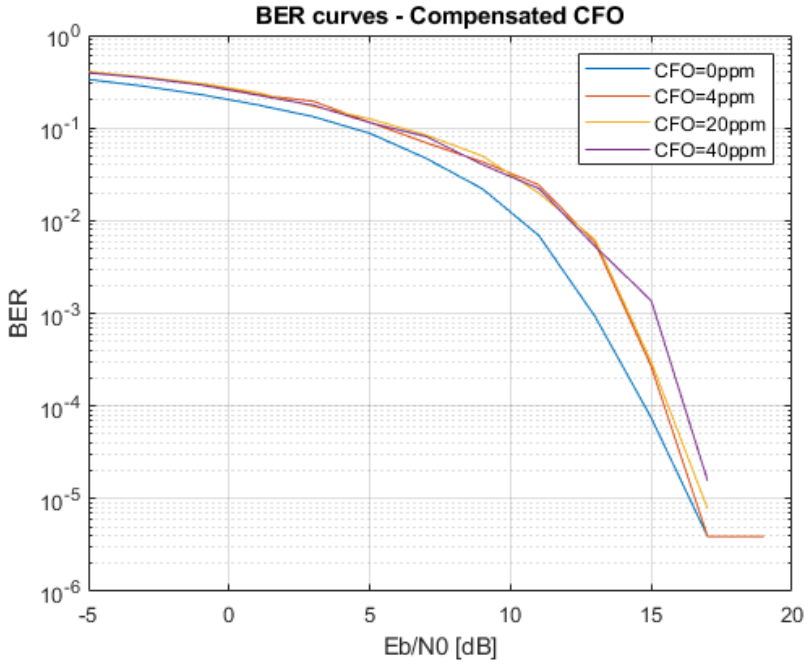

Figure 28: BER curve of compensated CFO using frequency tracking

3 SIMO Communication

3.1 Beamforming

The beamforming method is the process of searching for the angular distribution of the incident waves around a local area. The angular distribution around a local area for a tap n is deduced from the following equation:

$$a_n(\theta,\phi) = \frac{\sum_i h_i(n) B_i^*(\theta,\phi)}{\sum_i |B_i(\theta,\phi)|^2} \tag{23}$$

a_n denotes the angular distribution of a set of incident waves at tap n. In this equation, i is the spatial index of an antenna in the local area. (θ,ϕ) is the angular direction of arrival, h is the channel impulse response. $B_i(\theta,\phi)$ is the function specifying how the phase of a wave evolves depending of the antenna's position for a direction of arrival (θ,ϕ).

$$B_i(\theta,\phi) = e^{-j\vec{\beta}\vec{r}_i} = e^{-j\frac{2\pi}{\lambda}(X_i sin\theta cos\phi + Y_i sin\theta sin\phi + Z_i cos\theta)} \tag{24}$$

It is possible to compute the angular distribution with the values of the channel impulse response calculated at the beginning of this project.

The angular spectrum is computed for the LOS scenario and for the NLOS scenario. For the LOS scenario, the LOS component is visible at the center of the distribution on figure 29(a). The NLOS case does not show any dominant LOS component in 30(a). These are the angular spectrum for a narrow bandwidth. For the wideband case, the angular spectrum of the first tap are displayed in figure 31(a) and 32(a) for the LOS case and for the NLOS case respectively.

The most important directions of the angular spectrum are represented by the blue dots on the figures. These peaks will serve to define a set of incident waves for each taps. This set of incident waves allows the building of a channel model for each channel with spatial index i.

3.2 Channel Model

A new channel model can be built for each tap n based on the selected peaks of the angular distribution.

$$\hat{h_i}(n) = \sum_{(\theta,\phi)} a_n(\theta,\phi) e^{j(\phi_i - \vec{\beta_k}\vec{r_i})} \tag{25}$$

ϕ_i is random variable that belongs to a uniform distribution between 0 and 2π. $\vec{\beta_k}$ is the wave vector relative to the considered direction of arrival.

This equation estimates the channel transfer function for a spatial index i and tap n. A SIMO communication with N antennas at the receiver can be simulated. Therefore,

N channels corresponding to the N antennas must be computed.

It will be seen that the SIMO communication harnesses the spatial correlation between antennas to allow spatial diversity. The placement of the antennas must be chosen carefully.

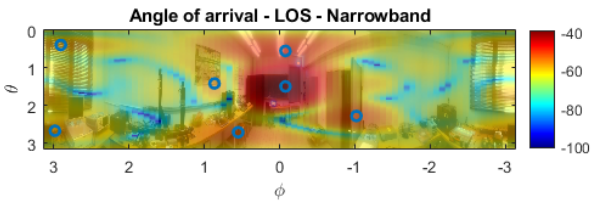

(a) Angle of arrival

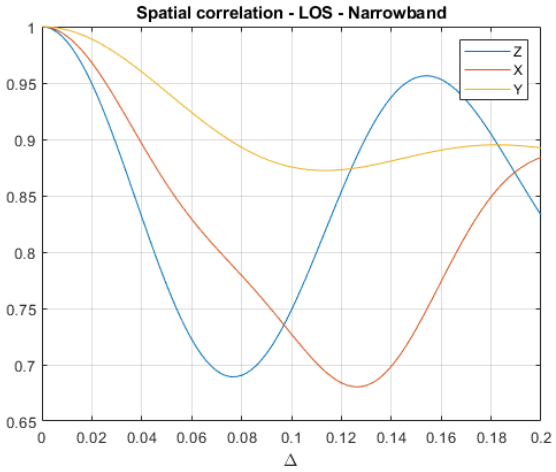

(b) Spatial correlation

Figure 29: Angular spectrum - Narrowband LOS channel model

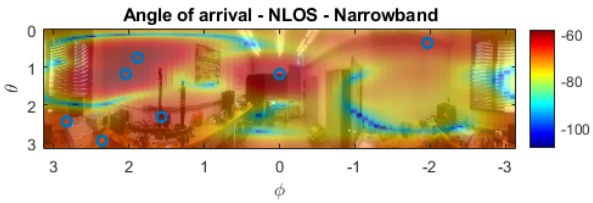

(a) Angular spectrum

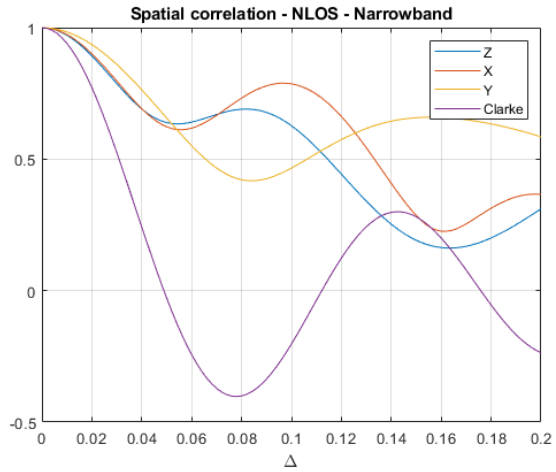

(b) Spatial correlation

Figure 30: Angular spectrum and Spatial correlation - Narrowband NLOS channel model

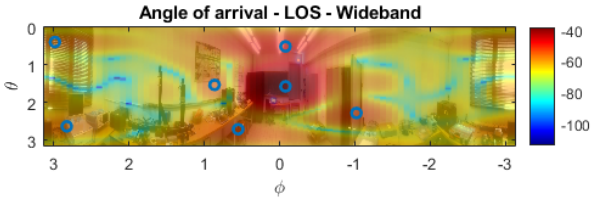

(a) Angular spectrum

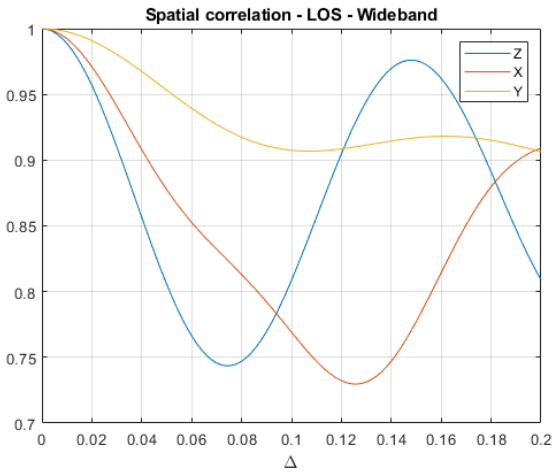

(b) Spatial correlation

Figure 31: Angular spectrum and Spatial correlation - Wideband LOS channel model

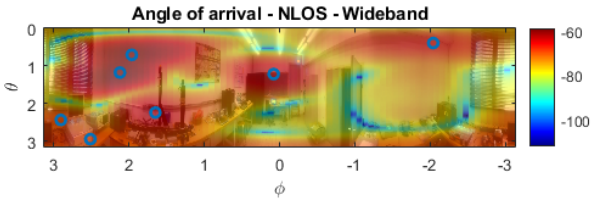

(a) Angular spectrum

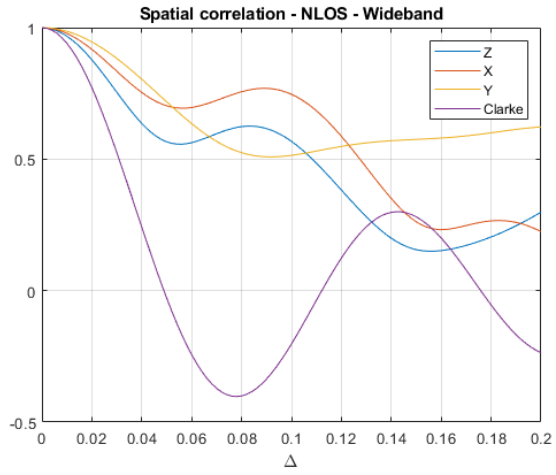

(b) Spatial correlation

Figure 32: Angular spectrum and Spatial correlation - Wideband NLOS channel model

3.2.1 Spatial correlation

To allow spatial diversity, the antennas must be placed some spatially uncorrelated point in space.

The spatial correlation for each dimension is found from the definition of the spatial correlation and the angular spectrum.

For the z direction:

$$R(\Delta z, n) = \sum_{i=1}^{N} |a_{z,n}(\theta)|^2 e^{j\beta cos\theta \Delta z} \tag{26}$$

$a_{z,n}(\theta)$ is the angular distribution around the z axis for tap n. It was calculated by averaging the angular distributions for which their respective direction of arrival yield the same value of $cos\theta$.

$$R(\Delta y, n) = \sum_{i=1}^{N} |a_{y,n}(\theta)|^2 e^{j\beta sin\theta sin\phi \Delta y} \tag{27}$$

$a_{y,n}(\theta)$ is the angular distribution around the z axis for tap n. It was calculated by averaging the angular distributions for which their respective direction of arrival yield the same value of $sin\theta sin\phi$.

$$R(\Delta x, n) = \sum_{i=1}^{N} |a_{x,n}(\theta)|^2 e^{j\beta sin\theta cos\phi \Delta x} \tag{28}$$

$a_{y,n}(\theta)$ is the angular distribution around the z axis for tap n. It was calculated by averaging the angular distributions for which their respective direction of arrival yield the same value of $sin\theta cos\phi$.

The results of the computed spatial correlation are displayed for the LOS case and NLOS case. The spatial correlation for the LOS case shows little variation between the narrowband case, figure 29(b), and wideband case, figure 31(b). This is expected since the narrowband is the results of the summation of the wideband taps. The LOS component being at the first taps of the wideband channel response leads to a less important contribution of the following taps.

The spatial correlation for the NLOS case, however, shows more variation between narrowband case, figure 30(b), and wideband case, figure 32(b). The LOS component is less imoprtant in this scenario, leading to different spatial correlations for the narrowband case and the first tap of the wideband case.

These correlation were obtained by considering only a finite number of incident waves. The commonly known Clark model assumes an infinite number of MPCs incident on the local area. The Clark model is dispayed as a comparison with the NLOS cases in figure 30(b) and 32(b). The Clark model shows correlation values equal to zero. This is not the case for the computed correlations. The performance brought by the spatial diversity will be lower for this real-world case than the ideal case. The computed correlations are still used to increase the performance of the communication. The antennas are placed based on the correlations value.

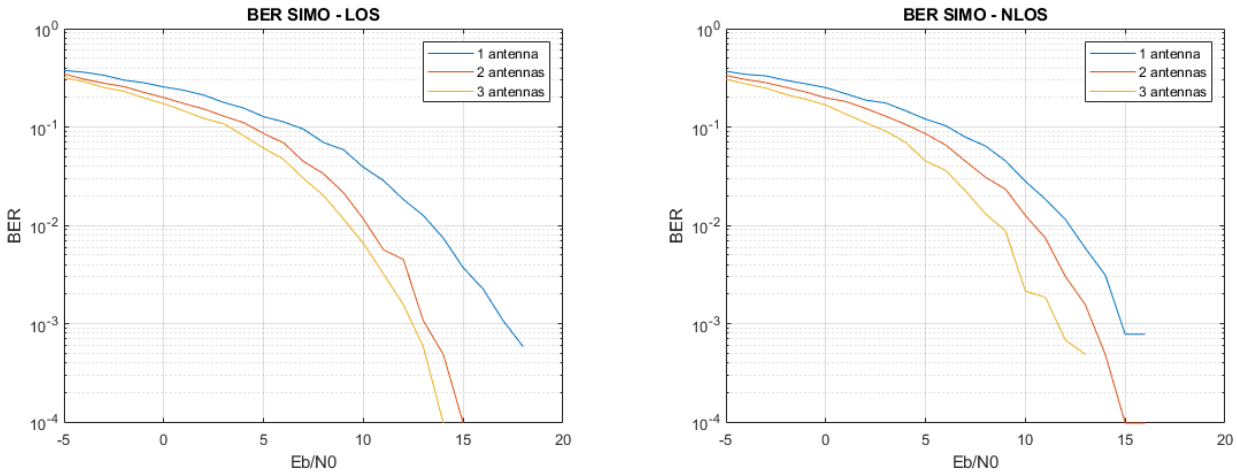

(a) LOS (b) NLOS

Figure 33: Evolution of BER with channel number

Now that the new channel model is built, a SIMO system can be implemented. A SIMO communication system is used to prevent the communication from the channel fading. Since the fading is the result of MPCs interfering constructively and destructively, the signal can be of poor quality and reduce significantly the BER performance. When using multiple antennas, multiple versions of the received signal are treated. Therefore, the probability that several received signal undergo a high fading is reduced significantly.

One way to recover the sent symbols is to average the received signals by the different antennas placed in the local area.

$$\hat{S}(k) = \frac{1}{N}\sum_{i=1}^{N}\frac{R_i(k)}{H_i(k)} = \frac{1}{N}\sum_{i=1}^{N}S_i(k) + \frac{W_i(k)}{H_i(k)} \tag{29}$$

N is the number of considered antennas. The problem with this approach is that some channels attenuates noise better than the other channels. The maximum ratio combining (MRC) is a better option. This method consists in a weighed sum where a term relative to a channel with attenuated noise has more importance. The MRC is a method of spatial diversity that is expressed as follows.

$$\hat{S}(k) = \sum_{i=1}^{N}\frac{H_i(k)^* R_i(k)}{\sum_{j=1}^{N}|H_i(k)|^2} \tag{30}$$

$$\hat{S}(k) = \sum_{i=1}^{N}\frac{H_i(k)^* H_i(k) S(k)}{\sum_{j=1}^{N}|H_j(k)|^2} + \frac{H_i(k)^* W_i(k)}{\sum_{j=1}^{N}|H_j(k)|^2} \tag{31}$$

The figure 33(a) displays the BER for different numbers of antennas. The BER performance is increased as the number of antenna increases. The probability that the all

antennas suffers highly from fading is reduced, hence, the increase of performance.